Twin-boundary and stacking-fault energies in Al and Pd

Jian-hua Xu* and W. Lin
Department of Physics and Astronomy, Northwestern University, Evanston, Illinois 60208-3112

A. J. Freeman
Department of Physics and Astronomy, Northwestern University, Evanston, Illinois 60208-3112
and Argonne National Laboratory, Argonne, Illinois 60439-4843
(Received 27 August 1990)

The (111) twin-boundary and stacking-fault energies of aluminum and palladium were investigated with use of the all-electron total-energy linear muffin-tin orbitals method based on the local-density approximation. Fault energies are determined by comparing the total energies obtained for the same-size supercells for each of two cases (with and without fault). The calculated values of the twin, intrinsic, and extrinsic fault energies, 130±15 (97±5), 270±50, and ~330 ergs/cm^2 for aluminum (palladium) are generally 30% larger than experiment. This discrepancy between the calculated and observed values may be attributed to the neglect of relaxation, the effect of the (finite) size of the supercell (at most 28 atoms/cell), and/or the use of the local-density approximation. Our calculated results appear to verify the correctness of the empirical relationship $2E_{tw} \simeq E_{SF}$, where E_{tw} and E_{SF} are the twin and stacking-fault energies, respectively.

I. INTRODUCTION

Twin and stacking-fault energies (in the broad sense, interfacial energies), have intrigued many metallurgists and solid-state physicists for years because of their importance for determining many physical properties. Thus, for example, it is well known that the mechanical properties are closely related to the existence of twin or stacking faults in alloys.[1] Despite the fact that a large amount of experimental data about twin and stacking-fault energies have been accumulated for pure metals,[2] there are still large uncertainties in the measured values of such interfacial energies. For example, the values of the twin energy for Cu range[1] from 20–160 ergs/cm^2. Direct measurements of these interfacial energies require very delicate techniques (such as the weak-beam electron microscopy method) to measure an extended single dislocation. Moreover, the measured value of such an interfacial energy depends sensitively upon many factors, such as the existence of internal stresses, impurities in the matrix (which are experimentally very difficult to control), temperature, etc. Nevertheless, experimental data show that the relation $2E_{tw} \simeq E_{SF}$ generally holds[1] to within an accuracy of 25%, where E_{tw} and E_{SF} are the twin and stacking-fault energies, respectively. Similarly, the theoretical values of twin and stacking-fault energies obtained by the pseudopotential method[3,4] are quite dispersed; in addition, the calculated values are, in general, lower than experiment. Thus, it appears worthwhile to study twin and stacking-fault energies and to determine their values from first-principles all-electron calculations. Very recently, a first-principles study of the intrinsic stacking fault in face-centered cubic metals was reported by means of the layer Korringa-Kohn-Rostoker (LKKR) method.[5] These authors studied the electronic structures of (111) twin stacking faults in Cu, Ir, and Al, and succeeded in reproducing the experimental trend of the twin-fault energy for Cu, Ir, and Al.

In the present work,[6] we employed a total-energy approach based on Hohenberg-Kohn-Sham local-density-functional theory[7] to study the electronic structure and energies of twin and stacking faults, namely the all-electron self-consistent linear muffin-tin orbitals (LMTO) method in the atomic-sphere approximation (ASA).[8] Overall, the calculated fault energies for pure aluminum and palladium yield the right order of magnitude, but are 30% larger than experiment. This appears to be the correct trend for the model employed since the relaxation around the fault region may contribute to lower the fault energy, especially in the stacking-fault case. The calculated twin energy and the overall density of states for Al are in fairly good agreement with the results of Ref. 6. Moreover, the calculated results appear to show the correctness of the experimental finding[1] that $2E_{tw} \simeq E_{SF}$.

II. METHODOLOGY

It is well known that in the fcc crystal the fault planes, which are also the glide plans, are the close-packed (111) planes. The close-packed fcc structure can be generated by stacking these close-packed layers on top of one another along the [111] direction in the (normal) sequence $\cdots ABCABC \cdots$ [Fig. 1(a)]. Twins and stacking faults are considered to be the two kinds of simplest stacking disorder: the twin orientation means that atomic positions above and below the fault plane are related to each other via a 180° rotation or a mirror plane reflection, i.e., $\cdots ABCACBA \cdots$ [Fig. 1(b)]. The stacking faults can be further classified as intrinsic and extrinsic—two categories suggested by Frank.[1] The intrinsic (extrinsic) stacking fault may be created in a fcc crystal by removing

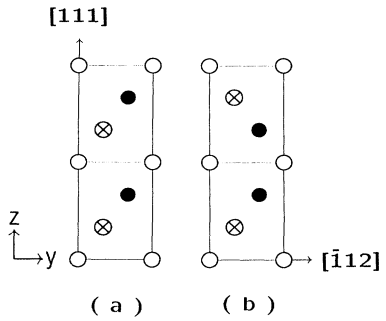

FIG. 1. Vertical sideview of a unit cell for (a) fcc and (b) twin-boundary configurations stacking along the [111] direction. Open, crossed, and solid circles denote A, B, and C layers, respectively.

ing (inserting) part of a close-packed plane, as shown in Figs. 2(a) and 2(b). Alternatively, the stacking fault can be formed by a shear on the (111) planes along the $[\bar{2}11]$ direction with a vector $\frac{1}{6}[\bar{2}11]$, and displacements $A \rightarrow B$, $B \rightarrow C$, and $C \rightarrow A$ relative to positions on the original plane. The intrinsic and extrinsic stacking faults can be represented in the notation $\cdots ABCBCABC \cdots$ and $\cdots ABCBABC \cdots$, respectively. A distinguishing common feature for both intrinsic and extrinsic stacking faults is that there is a local hcp environment around the fault plane, and the relaxations may occur around the fault region [for instance, removal (or insertion) of part of the close-packed plane (cf. Fig. 2)].

In our calculations, we preserved the close packing in the fault crystal, and only considered the stacking order difference (i.e., stacking disorder) along the [111] direction. For simplicity, the model of the stacking fault is

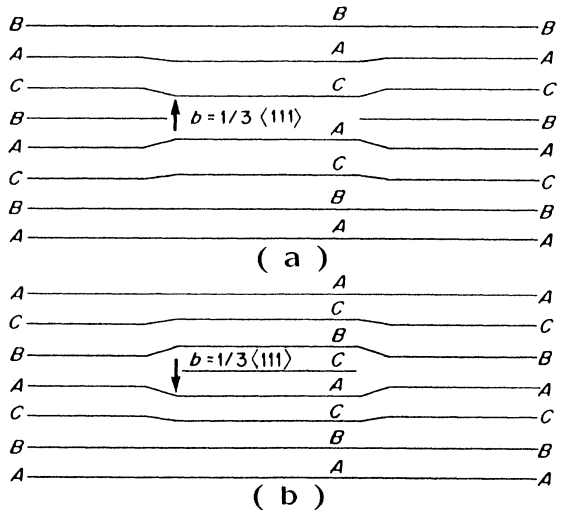

FIG. 2. (a) An intrinsic stacking fault formed in a fcc crystal by removing part of a close-packed plane. (b) The addition of an extra close-packed plane to a fcc crystal produces an extrinsic stacking fault (both after Ref. 15).

formed by removing (inserting) one whole close-packed (111) layer [cf. Figs. 3(a) and 3(b)]. Figures 1(a) and 1(b), and Figs. 3(a) and 3(b) represent a side view of the supercell of the fcc, twin (tw), and intrinsic and extrinsic stacking faults (ISF and ESF), respectively; Fig. 4 shows the top view (or bottom) of the (rectangular) supercell. Note that we prefer to choose the rectangular bottom instead of the primary (rhombus) one because we found that, using the linear tetrahedron scheme, better accuracy of the total number of electrons is obtained. Each supercell contains 12, 20, and 28 atoms for twin, ISF, and ESF, respectively.

The fault energy is simply defined as the total-energy difference between fault and perfect crystal. Note that the fault energy, which has a value of order 10^{-5} to 10^{-7} of the total energy, is obtained by subtracting two total energies (with and without fault); therefore, we must be cautious and obtain highly precise total energies. Now, it is well known that the total energy depends upon the number of $\mathbf{k}$ points sampled within an irreducible wedge of the Brillouin zone (IBZ), and the shape and size of the IBZ. In principle, for obtaining reliable values of such interfacial energies an accurate value of the total energy extrapolated to an infinite number of $\mathbf{k}$ points in the IBZ is required.[9] However, owing to the large supercell employed, we are capable of carrying out the calculations by sampling only a few hundred $\mathbf{k}$ points within the IBZ. Therefore, we studied not only the dependence of the total energy on the number of $\mathbf{k}$ points, but also compared the total energies of perfect and fault systems as obtained from two unit cells having exactly the same size and shape and use the same (finite) number of $\mathbf{k}$ points to eliminate systematic errors.

Relaxation and entropy contributions are not taken into account in the calculations, and we assume that stacking faults in neighboring cells do not interact with each other. The core states are treated fully relativistically and the valence states semirelativistically (i.e., omitting the spin-orbital interaction). Self-consistency was assumed when the deviation between input and output potential was less than 1 mRy. The Hedin-Lundqvist formula was adopted for the exchange and correlation potential.[10] The tetrahedron integration scheme[11] is em-

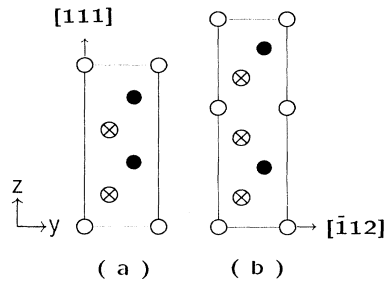

FIG. 3. Vertical side view of a unit cell for (a) the intrinsic and (b) extrinsic stacking fault along the [111] direction; a double-sized cell is adopted in the calculation for comparison with the same size hcp-structured supercell. Open, crossed, and solid circles denote A, B, and C layers, respectively.

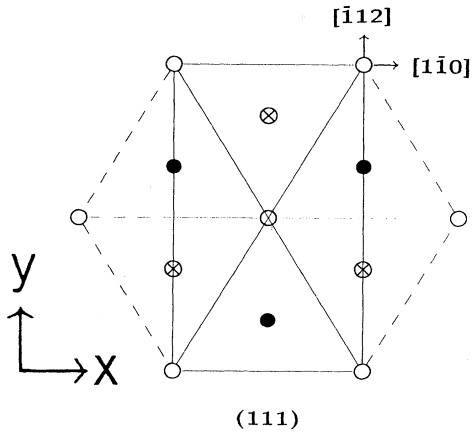

FIG. 4. Bottom of rectangular unit cell in the closed-packed (111) plane.

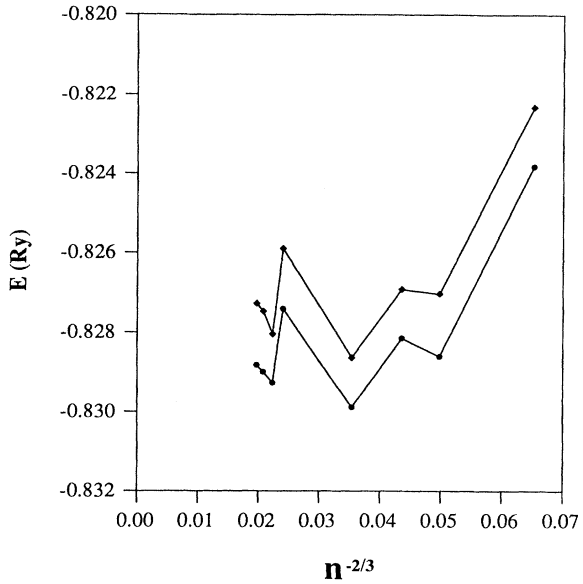

FIG. 5. Dependence of the total energy (from which −483 Ry/atom has been subtracted) (Ry/atom) vs $n^{-2/3}$ for Al, where n is the number of k points in the linear tetrahedron scheme. Solid circle and rhombus denote fcc and twin boundary supercell configurations, respectively.

ployed to obtain the density of states. The charge distributions are constructed using the "pseudo-muffin-tin-orbital" (pseudo-MTO) procedure[12] in which the spherically symmetric potential and charge obtained from the previous self-consistent results were employed to construct pseudo-MTO's and then the pseudo-MTO charge density in the whole space (including the interstitial region) is plotted as contour curves.

III. RESULTS

It is known that, in the linear tetrahedron k-space integration scheme, the total energy varies with the number of **k** points as (Ref. 9) $n_k^{-2/3}$, where n_k is the number of **k** points in the irreducible wedge of the BZ. Figure 5 exhibits the variation of the total energy of Al versus $n_k^{-2/3}$ in the fcc and twin supercells. It is expected that the larger the number of **k** points adopted in the calculation the lower the value of the total energy obtained. However, up to $n_k = 362$, the total energy still fluctuates with the number of **k** points ($n_k^{-2/3}$) within 2.5 mRy/atom. Therefore, it appears at a first glance that we cannot obtain the fault energy by simply subtracting the total energy (per atom) of the fault system from that of the perfect fcc cell Al. However, the energy difference between the twin and the fcc-structured supercells remains nearly constant (within 0.3 mRy/atom) for $n_k > 90$. Therefore, the twin-fault energy can be readily obtained from the energy difference of these two supercells using the same finite number of **k** points. Thus, as stated above, the purpose of choosing the same-size supercell for both twin and fcc structures in order to eliminate any systematic error seems to be accomplished.

Likewise, the value of the ISF total energy fluctuates with the number of **k** points, as shown in Fig. 6. Therefore, based on the same strategy, we evaluate the ISF energy by subtracting the two total energies (with and without fault) obtained from the two same-size supercells. However, in the SF case we chose the same-size hcp-structured supercell instead of the fcc-structured supercell to produce a cancellation of systematic errors, because it is computationally easier to choose a relatively small-size hcp-structured than a fcc-structured supercell. But in order to obtain the SF energy we need to compare the total energy of the fault system with that of the fcc-structured supercell. Hence, we make use of the parallel

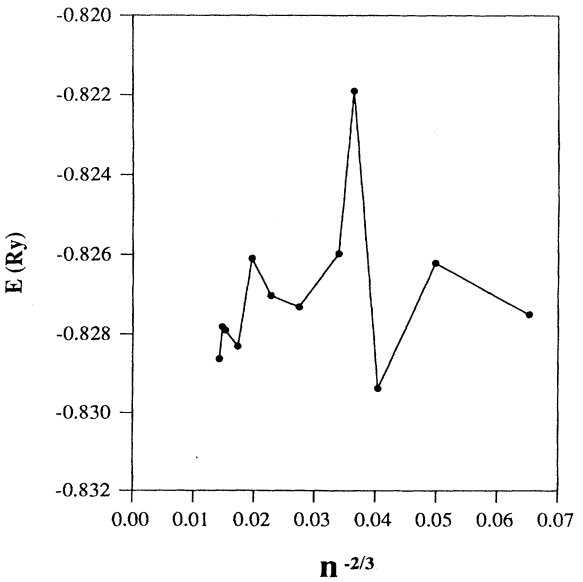

FIG. 6. Dependence of the total energy (from which −483 Ry/atom has been subtracted) (Ry/atom) vs $n^{-2/3}$ for Al in intrinsic stacking-fault configuration (see Fig. 5).

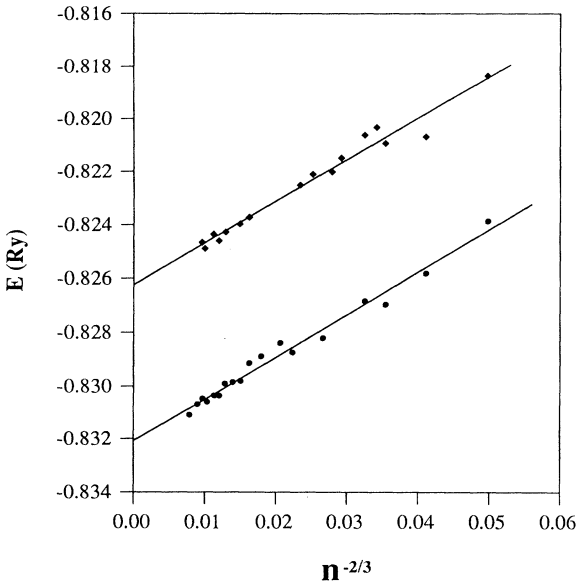

FIG. 7. Dependence of the total energy (from which −483 Ry/atom has been subtracted) (Ry/atom) vs $n^{-2/3}$ for Al. Solid circle and rhombus denote fcc and hcp primary cells, respectively.

dependence of the total energy versus $n^{-2/3}$ (up to $m_k = 1440$) between primary cell fcc- and hcp-structured Al (cf. Fig. 7). After extrapolating to an infinite number of **k** points, the total energy (per atom) of hcp Al is about 5.8 mRy higher than that of fcc Al (Fig. 7). Therefore, the SF energy $E_{SF} = (E_{SF} - E_{hcp}) - (e_{hcp} - e_{fcc})N$, where E_{SF} and E_{hcp} denote the calculated total energy of SF and hcp supercell, respectively, and e_{hcp} and e_{fcc} denote the total energy per atom of hcp and fcc primary cells, respectively. N denotes the number of atoms contained in the supercell. However, the error bar in the stacking-fault energy increases due to the second term in the above formula, which turns out to be N times the error of $(e_{hcp} - e_{fcc})$.

The calculated twin and SF energies for Al and Pd are listed in Table I.[13–16] The calculated intrinsic fault energy (280±40 ergs/cm^2) for Al has approximately the same value as the extrinsic one (~260 ergs/cm^2). It is expected from their structural arrangement, i.e., in ISF (or ESF), a layer is removed (or added) into the otherwise normal sequence along the [111] direction. We still do not understand the experimental trend, i.e., the extrinsic fault energy for Al is approximately 25% higher than that of intrinsic fault (cf. Table I). As seen, our calculated results appear to provide the support for the experimental finding that $2E_{tw} \sim E_{SF}$ (Ref. 1) for both Al and Pd. Moreover, the calculated twin energy (130±15 ergs/cm^2) is in fairly good agreement with the result of Ref. 5 (118 ergs/cm^2) obtained from the LKKR method; however, it is, in general, 30% larger than that observed value (extrapolated to 0 K) for Al. A possible reason for the discrepancy between the calculated and experimental values might be attributed to (i) neglect of the relaxation around the fault region, (ii) effect of the (finite) size of the supercell (or of neglecting the interactions between the two faults), and/or (iii) use of the local-density approximation. (We should note that we have found a similar overestimated value for the calculated antiphase boundary energy for NiAl.[17])

In order to understand the stacking disorder from the microscopic viewpoint, we inspect the electronic structures of fcc Al and Pd with and without faults. Figure 8 plots the density of states (DOS) for various stacking configurations (such as twin, ISF, and ESF, etc.) of Al and, for comparison, the DOS of pure fcc- and hcp-structured Al. Note that the general features (bandwidth and peak positions) of the DOS of Al in the twin configuration resembles that of the fcc structure; in particular the Fermi level lies on a dip of the DOS and only one prominent change (a peak) in the DOS twin can be seen in the energy region above 1 eV below E_F. Further, the density of states at E_F ($\simeq$0.3 states per eV atom) for the twin is not visibly modified compared with the fcc configuration. On the other hand, the DOS at E_F increases to $\simeq$0.4 states per eV atom for Al in the ISF or EFS configurations, because then the Fermi levels lie on a small but prominent peak of the DOS (instead of a dip), which might imply an instability. In fact, it merely reflects a local hcp structure contribution to the DOS [existing in the SF, cf. Fig. 8(e)]. Note that the overall features of the DOS of Al in the twin configuration (especially the peak positions near E_F) agree qualitatively with those of Ref. 5 using the LKKR method except for the

TABLE I. Twin and stacking-fault energies for Al and Pd (in ergs/cm^2).

		Al			Pd	
		Twin	ISF	ESF	Twin	ISF
	This work	130±15	280±40	~260	97±5	
	Ref. 5	118				
Calc.	Ref. 13	57	145	130		
	Ref. 4	61	160	133		
	Ref. 14	55	142			
	Ref. 1	75	166			180
Expt.	Ref. 15	120	200			180
	Ref. 16	75–100	135	180		
0 K (extrapolated)	Ref. 2	100–125	160	200		

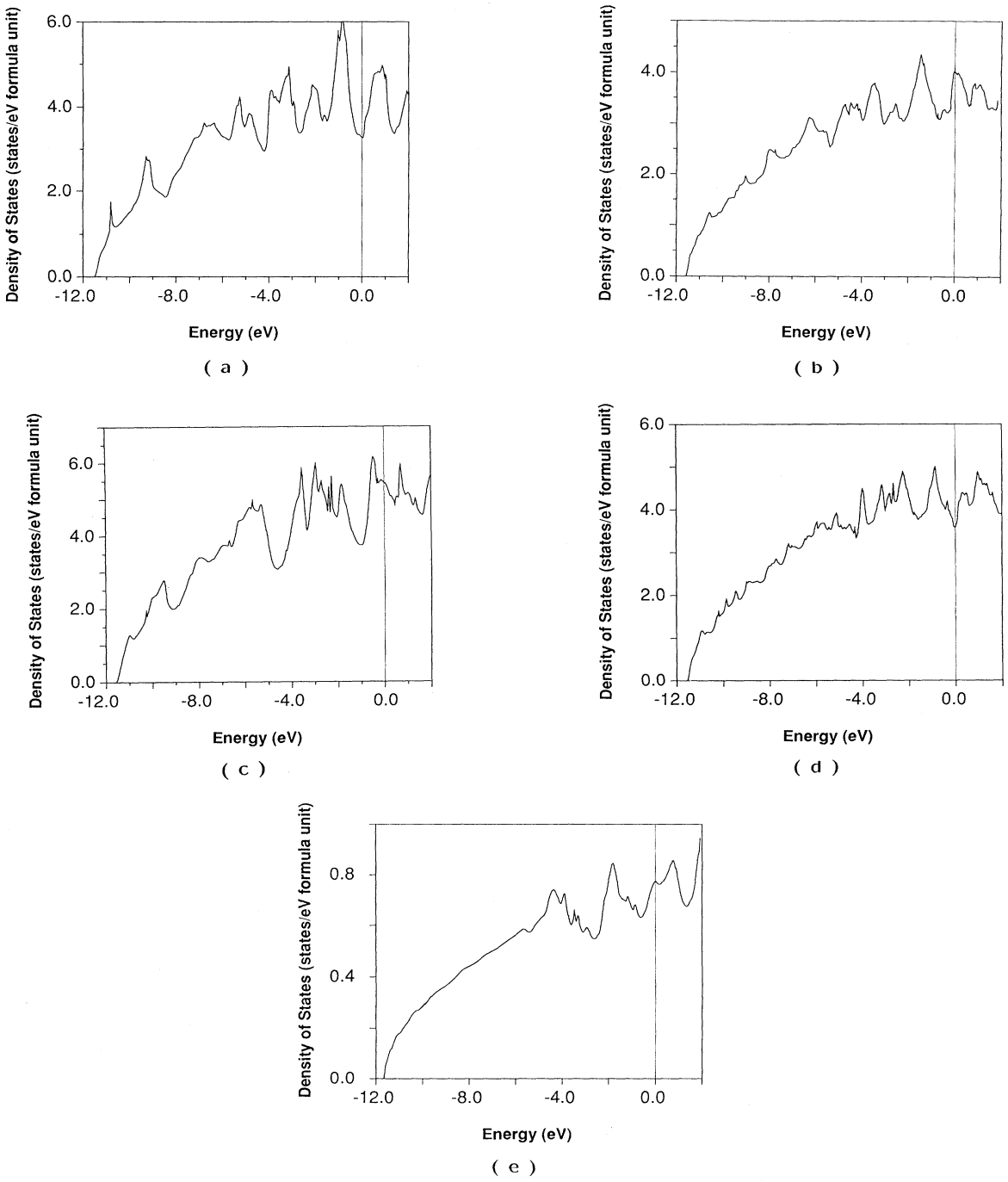

FIG. 8. Total density of states for Al: (a) twin boundary, (b) intrinsic stacking fault, (c) extrinsic stacking fault, (d) fcc supercell, and (e) hcp primary cell.

TABLE II. Total energy and its differences between the twin (or ISF) and fcc-structured supercell for Al, where $\Delta E_{tw} = E_{tw} - E_{fcc\ supercell}$, and $E_{ISF} = E_{ISF} - E_{fcc\ supercell}$ (in Ry/atom).

No. of k	Twin	ISF	fcc supercell	ΔE_{tw}	ΔE_{ISF}
90	−483.8270	−483.8262	−483.8286	0.0016	0.0024
300	−483.8280	−483.8270	−483.8296	0.0012	0.0023
362	−483.8273	−483.8261	−483.8288	0.0015	0.0027

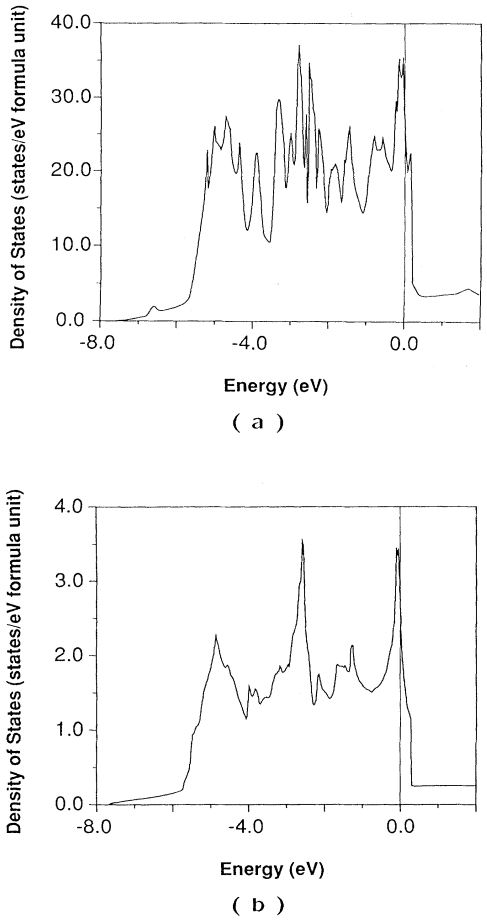

FIG. 9. Total density of states for Pd: (a) twin boundary and (b) fcc primary cell.

TABLE III. The number of kinks within a unit cell and the kink energy obtained from the twin, ISF, ESF, and hcp supercell (energy in ergs/cm^2).

	Twin	ISF	ESF	hcp supercell
Number of kinks	1	2	2	5
Single kink energy	130	140	~130	~200

location of E_F. Similarly, in the Pd case the general features (bandwidth and peak positions) of DOS for twin, cf. Fig. 9(a), is very similar to that of the fcc configuration, Fig. 9(b), except for several minor features appearing around the energy region 2 to 4 eV below E_F. The DOS at E_F is essentially not greatly altered for twin (32.7 states/eV formula-unit) as compared with the fcc-supercell (31.9 states/eV formula-unit).

As expected, the stacking disorder leads to a charge redistribution around the fault region. Figures 10 and 11 exhibit the valence charge-density contour plots for Al and Pd [in units of 10^{-3} electrons per (a.u.)^3] for twin and SF; for comparison, charge-density contour plots for the fcc and hcp structures are also included (Figs. 10 and 11). It is indeed seen that there is a marked charge accumulation (shaded region in Figs. 10 and 11) around the fault plane (or mirror plane) in the twin. (In contrast, no visible change was seen in the DOS at E_F for the twin as compared with the fcc supercell.) Moreover, note that the charge distortion is seen to be more profound in the SF case [Figs. 10(b) and 10(c)] than in the twin case [Fig. 10(a)] for Al, and more so in Al [Fig. 10(a)] than in Pd [Fig. 11(a)] for the twin case. This may explain, qualitatively, why the twin energy is smaller than that of the SF energy for Al, and why the twin energy of Pd is smaller

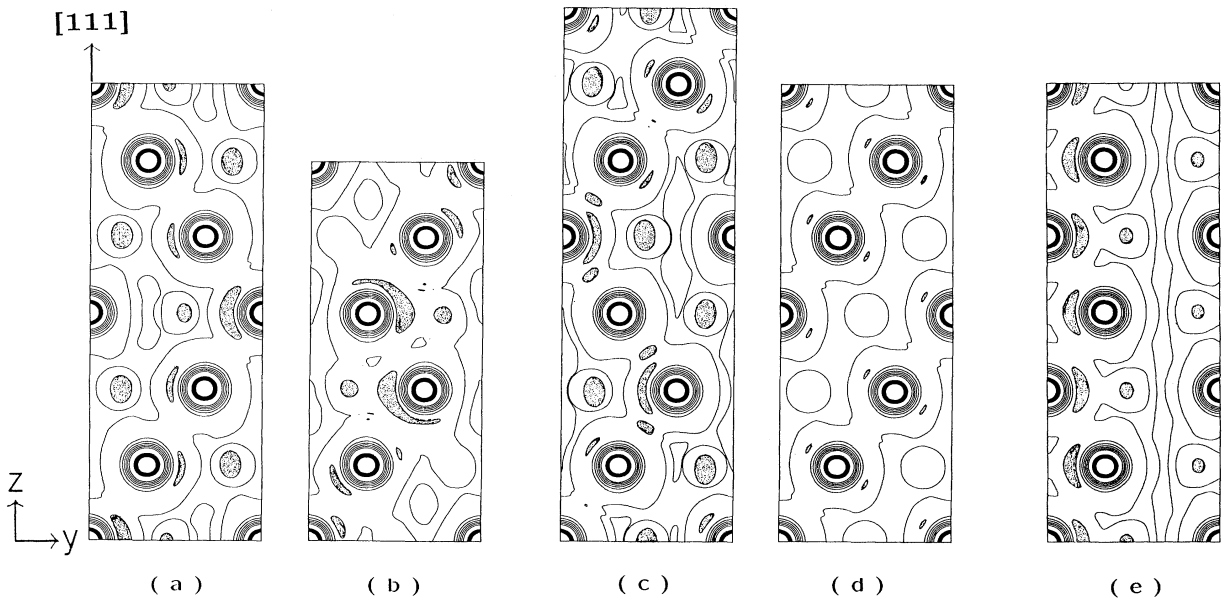

FIG. 10. Valence charge-density contours for Al: (a) twin boundary, (b) intrinsic stacking fault, (c) extrinsic stacking fault, (d) fcc supercell, and (e) hcp primary cell [linear scale, in units of 10^{-3} number of electrons/(a.u.)^3], where shaded regions denote high charge density [35×10^{-3} electrons/(a.u.)^3].

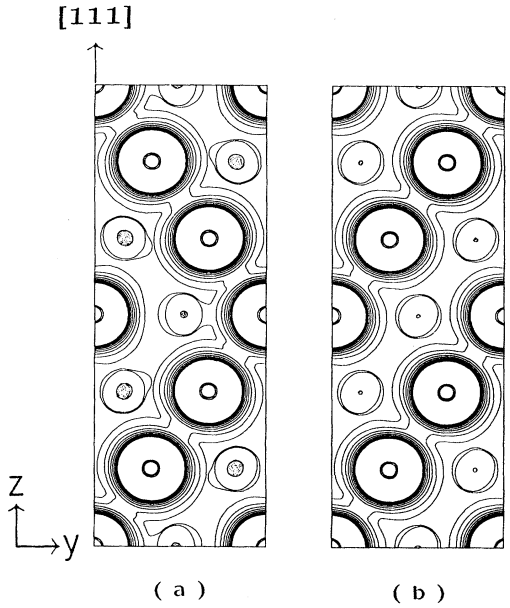

FIG. 11. Valence charge-density contours for Pd: (a) twin boundary and (b) fcc cell [linear scale, in units of 10^{-3} number of electrons/(a.u.)^3], where shaded areas denote high charge density.

than that of Al (cf. Table I).

One further remark is appropriate here: any fault (such as twin or SF, etc.) existing in an otherwise perfect fcc crystal structure can be viewed simply as introducing a different number of kinks along the [111] stacking direction. Furthermore, if we assume that the interaction between the two kinks is negligible, then the distinguishing feature between the twin and the SF is merely due to the difference in the number of kinks within a unit supercell. Table II lists the total energy (per atom) and its differences between the twin (or ISF) and the fcc-structured supercell for Al. Note that the energy difference between the ISF and the fcc-structured cell is nearly twice as large as that between the twin and the fcc-structured supercell. This can be understood in terms of the difference in the number of kinks, because there are one and two kinks within each cell for the twin and ISF, respectively. Now, a single kink energy can be defined as the fault energy divided by the number of kinks within a unit supercell. Table III lists single kink energies obtained from the twin, ISF, ESF, and hcp supercells. It is interesting to note that the energy for creating a single kink is roughly 130–200 ergs/cm^2 energy in pure fcc Al; obviously, since our calculated results may be overestimated by 30%, the kink energy may be in the range 100–150 ergs/cm^2, which to a certain extent verifies theoretically the observed range of coherent interfacial energies (up to about 200 ergs/cm^2).[18]

In fact, we have studied the fcc/hcp interfacial energy of pure aluminum using the simple model as *ABCABA* stacking along [111] direction, which is indeed equivalent to the ISF in removing a *C* layer from the normal sequence. The fcc/hcp interfacial energy for Al turns out to be $\sim$140 ergs/cm^2/interface. Note that the value of the kink energy also coincides with the energy difference between the hcp and fcc structures; as stated above, $e_{\rm hcp}-e_{\rm fcc}=5.8$ mRy/atom (i.e., $\sim$100 ergs/cm^2) for Al. In a sense, creating a kink in an otherwise perfect fcc crystal is nothing more than introducing a local hcp structure.

ACKNOWLEDGMENTS

This work was supported by the U.S. Air Force Office of Scientific Research (Grant No. 88-0346), by the U.S. Department of Energy (DOE), and by a computing grant at the DOE Office of Basic Energy Sciences (BES) computing facility at the National Energy Research Supercomputer Center (NERSC), LLNL. We are grateful to D. Wolf for stimulating discussions.

*Permanent address: Shanghai Institute of Metallurgy, Academy of Sciences of China, Shanghai 200050, People's Republic of China.

[1]J. P. Hirth and J. Lothe, *Theory of Dislocations,* 2nd ed. (Wiley, New York, 1982), p. 306.

[2]L. E. Murr, *Interfacial Phenomena in Metals and Alloys* (Addison-Wesley, New York, 1975).

[3]W. A. Harrison, *Pseudopotential in the Theory of Metals* (Benjamin, New York, 1966).

[4]J. P. Simon, J. Phys. F **9**, 1425 (1979), and references therein.

[5]S. Crampin, D. D. Vvedensky, J. M. Maclaren, and M. E. Eberhart, in *Atomic Scale Calculations in Materials Science,* edited by J. Tersoff, D. Vanderbilt, and V. Vitek (Materials Research Society, Pittsburgh, 1989), p. 141; J. M. MacLaren, S. Crampin, D. D. Vvedensky, and M. E. Eberhart, Phys. Rev. Lett. **63**, 2586 (1989).

[6]A preliminary report was given previously [J. H. Xu and A. J. Freeman, Bull. Am. Phys. Soc. **35**, 573 (1990)].

[7]W. Kohn and L. J. Sham, Phys. Rev. **140**, A1133 (1965).

[8]O. K. Andersen, Phys. Rev. B **12**, 3060 (1975); T. Oguchi and A. J. Freeman, J. Magn. Magn. Mater. **52**, 174 (1985).

[9]H. J. F. Jansen and A. J. Freeman, Phys. Rev. B **30**, 561 (1984).

[10]L. Hedin and Lundqvist, J. Phys. C **4**, 2064 (1971).

[11]J. Rath and A. J. Freeman, Phys. Rev. B **11**, 2109 (1979).

[12]N. E. Christensen, Phys. Rev. B **29**, 5547 (1984).

[13]P. Wilkes and C. M. Sargent, J. Mater. Sci. **6**, 216 (1972).

[14]J. F. Derlin and W. Bollmann, Phys. Status Solidi A **27**, K57 (1976).

[15]R. E. Reed-Hill, *Physical Metallurgy Principles,* 2nd ed. (Van Nostrand, New York, 1973), p. 892.

[16]R. E. Smallmann and P. S. Dobson, Metal. Trans. **1**, 2383 (1970).

[17]A. J. Freeman, T. Hong, and J.-h. Xu, in *Atomistic Simulation of Materials,* edited by V. Vitek and D. J. Srolovitz (Plenum, New York, 1989), p. 41.

[18]D. A. Porter and K. E. Eastering, *Phase Transformations in Metals and Alloys* (Van Nostrand Reinhold, United Kingdom, 1982), p. 113.